

Vacancy mediated magnetization and healing of a graphene monolayer

E. Nahkmedov^{1,2}, E. Nadimi³, S. Vedaei³, O. Alekperov², F. Tatardar^{2,4}, A. I. Najafov², I. I. Abbasov⁵, and A. M. Saletskii⁶

¹ Faculty of Physics, Moscow State University, Baku branch,
str. Universitetskaya 1, AZ-1144 Baku, Azerbaijan,

²Institute of Physics, Azerbaijan National Academy of Sciences, H. Cavid ave. 33, AZ1143 Baku, Azerbaijan,

³ Center for Computational Micro and Nanoelectronics (CCMN),
Faculty of Electrical Engineering, K. N. Toosi University of Technology, Tehran, Iran

⁴Khazar University, Mahsati str. 41, AZ 1096, Baku, Azerbaijan,

⁵ Azerbaijan State Oil and Industry University, Azadlig ave. 20, Baku, Azerbaijan

⁶ Faculty of Physics, Leninskie Gory 1-2, 119991 Moscow State University, Moscow, Russian Federation
(Dated: March 12, 2019)

Vacancy-induced magnetization of a graphene layer is investigated by means of a first principle DFT method. Calculations of the formation energy and the magnetization by creating the different number of vacancies in a supercell show that a clustering with big number of vacancies in the cluster is rather favorable than that of isolated vacancies, homogeneously distributed in the layer. The magnetic moment of a cluster with big number of vacancies is shown to be not proportional with the vacancy concentration, which is in good agreement with the recent experimental results. Our studies support the idea that although the vacancies in a graphene create a magnetic moment, they do not produce a magnetic ordering. It is shown that although the Lieb's rule for the magnetization in a hexagonal structure violates, two-vacancies, including a di-vacancy, in the supercell generate quasi-localized state when they belong to the different sublattices, and instead two-vacancies generate an extended state when they belong to the same sublattices. Analytical investigation of the dynamics of carbon atom- and vacancy-concentrations according to the non-linear continuity equations shows that the vacancies, produced by irradiation at the middle of a graphene layer, migrate to the edge of the sample resulting in a specific 'segregation' of the vacancy concentration and self-healing of the graphene.

PACS numbers: 74.78.-w, 74.62.-c, 74.70.Kn, 74.50.+r

I. INTRODUCTION

Investigation of graphene, the single two-dimensional (2D) sheet of graphite, is one of the priority direction among of allotropic modifications of carbon and related nanostructures due to its topological properties. Unusual properties of pristine graphene such as ballistic electron propagation with extremely high carrier mobility of $\mu_e = 10^4 \text{ cm}^2 \text{ V}^{-1} \text{ s}^{-1}$ at room temperature^{1,2}, existence of massless, chiral low-energy excitations, characteristic to Dirac fermions, observation of anomalous integer quantum Hall effect (IQHE) even at room temperature³, makes it an attractive material for electro-technical industry. Recent experimental and theoretical investigations show that a graphene sheet with vacancies heal themselves under thermal annealing or electric potential spanning⁴⁻¹⁶, so that the vacancies either migrate toward the crystal edge or form a big hole near extended defects like grain boundary or dislocation in the crystal. This property of the graphene may have a great impact to the graphene based electronic technology.

Defects engineering may enormously change kinetic and magnetic characteristics of graphene, extending a scope of its application in spintronics. The defects are usually produced as point defects, like substitutional- and interstitial- impurities and vacancies, either in the fabrication processes of a sample or by means of external factors, such as radiation or heavy-ion bombardment and

chemical doping of a sample (see, e.g. [17] for a review). The vacancies are formed in a crystal by reconstruction of the lattice as a result of knock-on of carbon atoms from the graphene lattice or/and as a result of bond rotations, e.g. the formation of Stone-Wales (55-77) and 8-ring defects, under bombardment with high-energy particles. A beam of the high-energy particles acts as a local heat source and thus helps to overcome the defect formation energy barrier. Note that a new class of the carbon-based materials has been experimentally revealed¹⁸, which has a nanoporous structure and it is catalytically active. The nanoporous carbon is less ordered than graphite but not completely amorphous. Theoretical studies have shown¹⁹ that an introduction non-hexagonal rings by means of vacancies into carbon structure most likely method to get a nanoporous carbon structure.

Although many effects observed in graphene are attributed to the presence of vacancies and defects, we will focus here particularly on a magnetic response and self-repairing of graphene in the presence of vacancies.

Magnetic response associated with vacancies produced by the irradiation of graphene with high-energy protons and carbon (C^{4+}) ions has been studied recently as experimentally²⁰⁻²² as well as theoretically²³⁻²⁹ by means of the molecular dynamics simulations and DFT based *ab-initio* methods. Many experimental observations reported in the literature provide inconsistent even contradictory results. Experimental evidence of ferromagnetic

order has been observed²¹ in irradiated graphene, the origin of which was suggested by the authors to be the defects located in the structure. Magnetic ordering was mainly observed in graphitic materials²², which was explained by the existence of the localized electronic states at grain boundaries of highly oriented defective pyrolytic graphite. Some observation of ferromagnetism even anti-ferromagnetism seems to be artifacts.

Ab-initio density-functional theory (DFT) investigations of magnetization produced by vacancies in a graphene are mainly performed^{19,24–30} by a superlattice method, where a vacancy is created in a supercell of the big number of unit cells, periodically extended with images of the original vacancy. Spin orientations in each supercell become the same, yielding seemingly a ferromagnetic signature of total magnetization even in the absence of a spin-spin interactions. Nevertheless, we believe that a magnetic ordering in a system should be achieved by exchange interactions between the magnetic moments. A numeric computation reveals that a vacancy in graphene^{20,31,32} introduces a semi-localized π -midgap state with Coulomb-like $\sim 1/r$ decay potential. The single-atom defects create in the graphene a quasi-localized state at the Fermi level^{32–35}. The graphene structure can be viewed as two interpenetrating hexagonal sublattices of carbon atoms labeled as *A* and *B* ones, forming a bipartite lattice. A defect introduced into the *A* sublattice results in a quasi-localized state due to the p_z orbitals of carbon atoms in the *B* sublattice and vice versa. A short-range repulsive Hubbard interactions between vacancies at higher concentrations and with half-filled band may result in a ground state with total spin $S = |N_A - N_B|/2$ according to Lieb's theorem³⁶, where N_A and N_B are the number of vacancies in *A* and *B* sublattices, correspondingly, of a bipartite lattice. The balance between N_A and N_B is destroyed at e.g. zigzag edges, which may provide a low-temperature background magnetism observed in a graphene sample³⁷.

Recent investigation of a graphene sheet by controllable doping it with fluorine adatoms and creation of vacancies by irradiation^{38–40} has indicated that both defects induce a magnetic moments with spin 1/2. Nevertheless, they do not result in a magnetic ordering, rather an induced paramagnetism down to liquid helium temperatures was observed in the doped samples. Low temperature measurements of pristine graphene by using SQUID magnetometry disclose strong diamagnetism⁴⁰, and show a tiny background paramagnetism, observable at $T < 50$ K. The samples under investigation were shown^{38,40} to consist of electronically decoupled 10–50 nm mono- and bilayer graphene crystallites, which are aligned parallel to each other. Evaluation of the spin number N from the measurement data shows that the number of paramagnetic center is proportional to the defect concentration x for a small concentration ($x < 0.5$), and the dependence is more complicated for higher concentrations. For each concentration x , the measured number of paramagnetic centers is three orders of mag-

nitude less than the measured number of defects in the samples. This experimental fact can be understood such that only one of out ~ 1000 defects contributes to the paramagnetism in contradictory to other experiments as well as *ab-initio* investigations^{19,24–27,29} that each defect contributes one Bohr magneton μ_B to the total magnetization. Note that the vacancy magnetism in graphene was recently shown³⁹ to be originated from two approximately equal contributions: one from the dangling bonds and other from itinerant magnetism.

High resolution transmission electron microscope (HRTEM) monitoring of a graphene sheet at 80 keV operating energy has displayed⁴ a formation of a hole, which seems to support the above described experiment³⁸ on vacancy magnetism. Indeed, as we will show, agglomeration of the vacancies in a big hole results in not a linear increase of the magnetic moment with vacancy concentration. Theoretical investigations of time-evolution of a graphene with dense vacancies by means of non-equilibrium molecular dynamics⁵ reveal also a tendency toward a formation of the haeckelites in the case with small number of the vacancies, while forming a large hole as the number of vacancies increases.

A systematic scanning transmission electron microscopy (STEM) study of a suspended graphene layer^{6,7}, deliberately introduced vacancies and deposited by metal atoms such as Cr, Ti, Pd, Ni, Al except for gold, shows that nanoscale holes were etched in the structure due to interactions of metal atoms with graphene. The nanoholes were observed at room temperature in ultrahigh vacuum (6×10^{-9} mbar) under low-energy 60 keV (lower than the threshold 'knock-on' energy 86 meV for a carbon atom⁸ in graphene) that electron-beam scanning acts as catalysts for etching holes on the graphene surface. Instead, the mending and filling of many-vacancy holes (over 100 vacancies) was observed⁹ in room-temperature metal-catalyzed etching STEM experiments under the same conditions described above, provided a reservoir of loose carbon atoms is readily available nearby holes. This process was interpreted by the authors as a dislodging of carbon adatoms from the graphene surface by the scanning electron-beam and dragging them to the edge of the holes, which results in refilling the holes by random combination of 5, 6, 7, and 8 carbon atom rings.

Healing effect in graphene, where the vacancies were produced by employing plasma bombardment¹⁰, has been performed by thermal annealing without external carbon atoms source in the temperature interval starting from 300°C up to 900°C. For higher temperatures the self-repairing was shown to stop. According to the results of Raman, x-ray photoemission spectroscopy (XPS), HRTEM, and electrical transport measurements the healing takes place by annihilation of displaced carbon atoms with vacancies with assistance of thermal energy. Healing was shown to become more difficult when the size of the vacancies' hole increases. Formation of monovacancy defects in the finite graphene flakes¹¹ and

graphene nanoribbons¹² was shown to be size-dependent, and that the vacancy defects migrate toward the edge at higher temperatures, as a result of which the structures heal themselves. DFT calculations and molecular dynamics simulations of the vacancy migration in graphene flakes show¹³ thermally activated motion of vacancy toward the edge occurs even at room temperature whereas the probability of return motion back to the middle is negligible.

Our *ab-initio* investigation of the vacancies and analytically study of their migration in a graphene layer supports the experimental results on magnetism measured in³⁸ as well as the experiments on self-healing of a graphene. Analysis of our calculation results shows that the formation energy and magnetization of divacancy is lower than those of single vacancies. Single vacancies are enough mobile, and they diffuse toward the extended defects like a grain boundary, a dislocation or a sample edge (which can be considered as an extended defect) or coalesce with other vacancies, forming poly-vacancies with lower energy and magnetic moment. We show that a merging of a single vacancy with polyvacancies, resulting in defect cluster or hole with bigger size, is energetically favorable. According to our calculations the formation energy of a even-fold vacancy like di- or tetra-vacancy is lower than odd-fold vacancies. Therefore, they are more stable. Magnetic moments of the clusters with minimal formation energies are lower too. The magnetic moment of the graphene is determined by edge structure of the vacancy clusters. So that only that defect on the e.g. A sublattice that has no counterpart on the B sublattice will contribute to the magnetization. The authors of Ref. [12] considered a hole of $N > 1$ multiple vacancies, concluded that the dangling bonds these structural defect is proportional to the circumference of the hole or to \sqrt{N} , and therefore its formation energy is also proportional to \sqrt{N} . In contrast we show that a multiple vacancy hole is structured in different modifications, and at least one of them possesses minimal dangling bonds and, consequently minimal magnetic moment. Thus, there is a tendency of clustering of vacancies into big holes, instead of homogeneous distribution of isolated vacancies over the system in the irradiation process. It is worthy to note that total energy calculations have been done in Ref. [30] for nanoholes of various sizes, containing up to 60 vacancies, in a big supercell with 288 carbon atoms in graphene by applying *ab-initio* DFT method. Although the number of possible holes for a given number vacancies N increases sharply with N , it is hard task to calculate all possible cluster structures with higher N . Nevertheless, the results of Ref. [30] yield extremely useful information on stability and magnetism of holes with a great number of vacancies.

Such kind of “*segregation*” seems to be a result of two-dimensional character of the graphene sheet where an off-diagonal long range order (ODLRO) is absent. The crystalline structure of the graphene is controlled by power-like order. Correlations of the vacancies seem to be man-

aged also with power-like order, which compete with correlations between the carbon atoms in the structure. In order to understand the vacancy hole formation and healing mechanism in a graphene layer, a phenomenological kinetic model is employed by us for a migration of carbon atoms through vacancies. This model has been implemented to numerical studies of a segregation problem under irradiation of binary alloys^{41–51}, where A - and B -type atoms diffuse over vacancies and interstitials. We simplified the segregation problem for diffusion of carbon atoms over vacancies in one-dimensional (1D) case, and solved analytically the non-linear differential equations for carbon atoms- and vacancies- concentrations. The obtained results show that a vacancy created, say in the middle of the sample, diffuses to the edge of the sample. We think that boundary of samples can be considered as an “extended defect” like dislocations, grain boundaries or a hole of a big size. Therefore, the vacancies diffuse and are incorporated, commonly say around extended defects in the sample.

The paper is structured as follow: the computational method, employed for our *ab-initio* calculations is described in the next Section II. Section III presents the obtained results of *ab-initio* DFT calculations. Section IV provides our analytic investigation of diffusion-segregation problem for carbon atoms through vacancies, and migration of the vacancies toward the sample boundary. Our conclusions and speculations are given in Section V.

II. COMPUTATIONAL METHODS

SIESTA code is employed^{52,53} in our spin-polarized DFT-based *ab-initio* calculations, where the standard double- ξ basis with polarization orbitals (DZP) is used. The generalized-gradient approximation (GGA) is utilized to calculate the exchange correlation term⁵⁴. The interaction between the valence electrons and the atomic core is taken into account by using standard norm conserving Troullier-Martins pseudopotential. The unit cell of a pristine mono-layer graphene is initially relaxed and then three different supercells of 50, 98, and 162 atoms are constructed. The real space integration grid had 200 Ry cutoff and 50 meV energy shift. Spin resolved calculations are performed in most cases. k -point sampling of the Brillouin zone was performed by using the Monkhorst-Pack method⁵⁵. In order to get an optimal self-consistency convergence, the density of electronic states (DOS) was calculated for different k -point meshing. Our calculations show that $5 \times 5 \times 1$ k -point mesh is a good and optimal choice to have a balanced accuracy and computation time. To obtain the equilibrium geometry we relaxed all the atoms after creation each vacancy until the forces acting on them were smaller than $0.01 eV/\text{\AA}$. The formation energy for mono-, di- and tri-vacancy are presented in Table I for the supercells with 50, 98, and 162 carbon atoms. The formation energy of

TABLE I: Formation energies of mono-, di- and tri-vacancy for the supercells with 50, 98, and 162 atoms.

Formation energy (eV)	1 vacancy	2 vacancies	3 vacancies
Supercell with 50 atoms	7.03	5.78	8.50
Supercell with 98 atoms	6.99	5.76	7.74
Supercell with 162 atoms	6.78	5.21	7.52

TABLE II: Formation energy and total spin polarization for the supercell of 98 atoms with different vacancies.

Type	Formation energy (eV)	Spin polarization ($Q_{up} - Q_{down}$)
Single defect	6.99	1.13
DV 5-8-5	5.76	0.0
DV 555-888	4.52	0.0
3 vac. 55-10	8.84	1.00
3 vac. 999-3	17.49	4.00
3 vac. 555-11	11.91	1.54
4 vac. 555-9	7.91	0.0
4 vac. 5-12-5a	11.27	2.02
4 vac. 5-12-5b	11.27	2.02
4 vac. 55-12	13.33	1.99
4 vac. 12-55	13.33	1.99

the vacancies changes slightly with the supercell size (see, Table I) as a result of interaction of the defects with their images in the neighboring auxiliary cells (we used periodic boundary conditions in all space directions). Our calculations of the formation energy, DOS, and the magnetization show that a good convergence can be reached for a supercell with at least 98 atoms. Therefore, our results presented below were done for a supercell with 98 atoms.

III. DISTRIBUTION OF THE VACANCIES AND THEIR MAGNETIZATION

Our aim in this investigation is to understand a development of the magnetization with increasing the vacancy concentration and a restructuring tendency due to the vacancies migration in the graphene mono-layer. We calculated for this purpose the formation energy, the band structure, and the DOS of a supercell of 98 atoms with up to four vacancies in different configurations. The $C-C$ bond length of a pristine graphene lattice is calculated to be 1.409 Å, 1.412 Å, and 1.412 Å for the supercells correspondingly with 50, 98, and 162 atoms, which is in good consistent with the experimental value of 1.42 Å. Creation of one vacancy, producing pentagon-nonagon type 5-9 defect in the supercell, results in the appearance of three dangling σ - bonds, two of which rebind again with each other due to the Jahn-Teller distortion around vacancy. Jahn-Teller distortion deforms the lattice around the vacancy and breaks the threefold symmetry; the ge-

ometrical distortion is relaxed off behind the vacancies. Covalent-bond coupling between two dangling bonds of the second-nearest-neighboring atoms belonging to the same sublattice stabilizes the vacancy extended states. The third dangling bond is left unsaturated and contributes $\approx 1 \mu_B$ in magnitude magnetic moment to the intrinsic magnetization. Removing one-, two- and three-carbon atoms located in the nearest-neighboring sites in the unit cell results in formation of correspondingly 5-9, 5-8-5, and 55-10 type defective configurations in the supercell (see, Fig. 1). DOS, the band structure, and the distributions of the deformation potential around the mono-, di-, and tri-vacancy distortions are depicted in Fig. 1. The deformation potential is seen to be significant within the unit cell around the vacancy. Therefore, interaction of vacancies through the distortion potential seems to be like to the dipole interaction and it would be important only for vacancies placed nearest-neighbor each other. The vacancies located far away each other may be considered practically as isolated vacancies. Formation energy of a single vacancy is calculated to be 6.99 eV (see, Table II). This result is slightly lower than those obtained by other authors $E_f \approx 7.5 \text{ eV}^{29,56,57}$, nevertheless it is in good consistency with the experimental data of $7.0 \pm 0.5 \text{ eV}^{58}$. The spin-polarized electronic band structures of a defective graphene with one vacancy and a pristine graphene are shown in Fig. 1a and Fig. 2a, correspondingly, for comparative study. The band gap of the perfect graphene is closed at the border of the Brillouin zone, yielding two Dirac cones. A single vacancy seems to remove the band crossing degeneracy at K -points of the Brillouin zone, and introduces at the same time two extended defect levels corresponding to spin-up and spin-down states at the Fermi level. Assuming that a continuous irradiation of a sample will create isolated vacancies, the magnetization of the sample would monotonically increase. Furthermore, in the absence of spin-spin correlations between localized dangling bonds, the magnetic moments of the vacancies belonging to different sublattice will partially compensate each other and reduce the total magnetization. Nevertheless, the magnetization under this assumption would monotonically increase with vacancy concentration. Our calculations below show that creation of mono vacancies monotonically distributed throughout the structure is not energetically favorable, and there is a tendency to form a cluster or hole of vacancies by coalescing them each other or collapsing around the extended defects like grain boundaries, dislocations or the sample boundary.

A divacancy (DV) is produced by the removal of two nearest-neighboring carbon atoms, composing the so-called 5-8-5 defect of an octagon and a pair of pentagons as it is shown in Fig. 1b. We calculated the formation energy of DV, presented in Table II, which is equal to $\epsilon_{DV}^f \approx 5.76 \text{ eV}$. *Ab-initio* calculations of the DV formation energy by other authors^{56,57} indicate $\sim 8 \text{ eV}$. The energy ϵ_{DV}^f is smaller than that for a monovacancy in a graphene, confirming that DV formation in the graphene

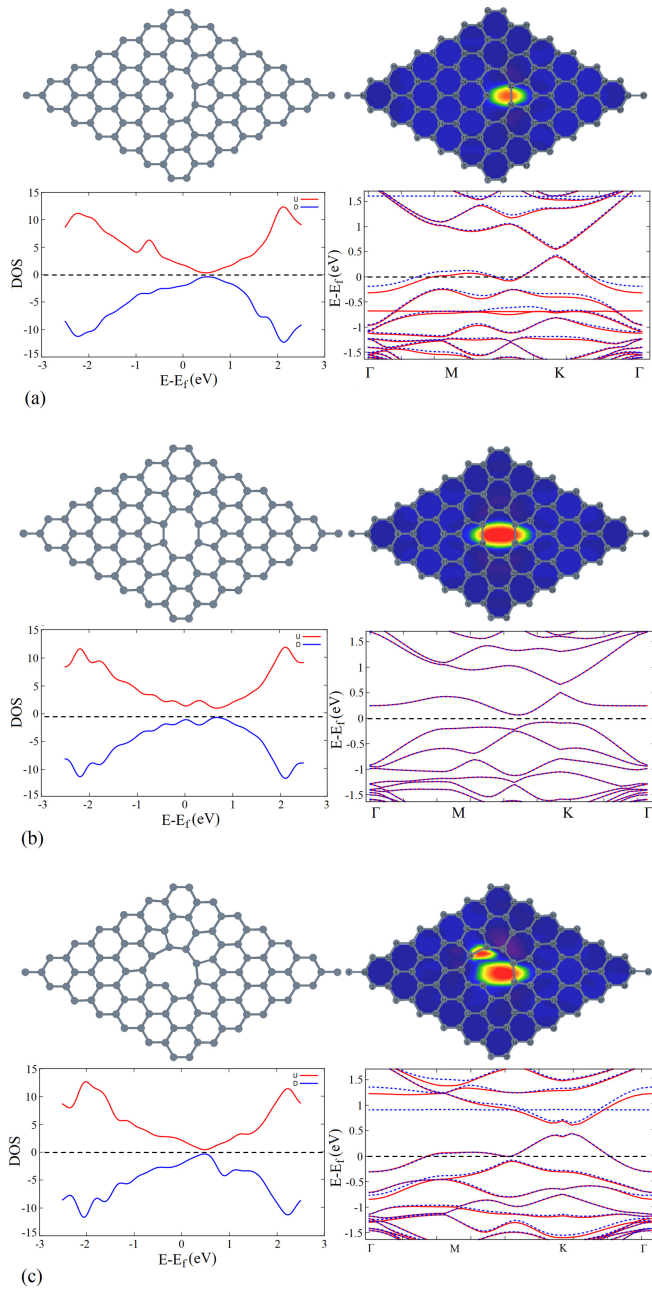


FIG. 1: The relaxed structure and the deformation potentials around the vacancies, the spin-polarized DOS and the band structures for (a) mono-, (b) di-, and (c) tri-vacancy, when one carbon atom or two and three nearest-neighboring carbon atoms are removed in the unit cell. The DOS, corresponding to spin-up and spin-down states, are plotted respectively by red- and blue-curves in opposite directions for clarity.

is rather favorable. Divacancies create a quasi-localized state with energies close to the Fermi energy E_F ; at the same time they remove the band crossing, destroying the gapless states at K -points of the Brillouin zone (see, Fig.1b). All the dangling bonds corresponding to the same sublattice rebind again, and therefore the DV

does not generate a magnetization (see, Table II).

The $5-8-5$ divacancy, consisting of two pentagons and one octagon, has another modification $555-777$, which is structured by three pentagons and three heptagons. The $555-777$ defect is formed by removing two carbon atom and by additional creation of a Stone-Wales (SW) defect⁵⁹, e.g. by additional rotation of one $C-C$ bond in the octagon. Although $555-777$ DV, with formation en-

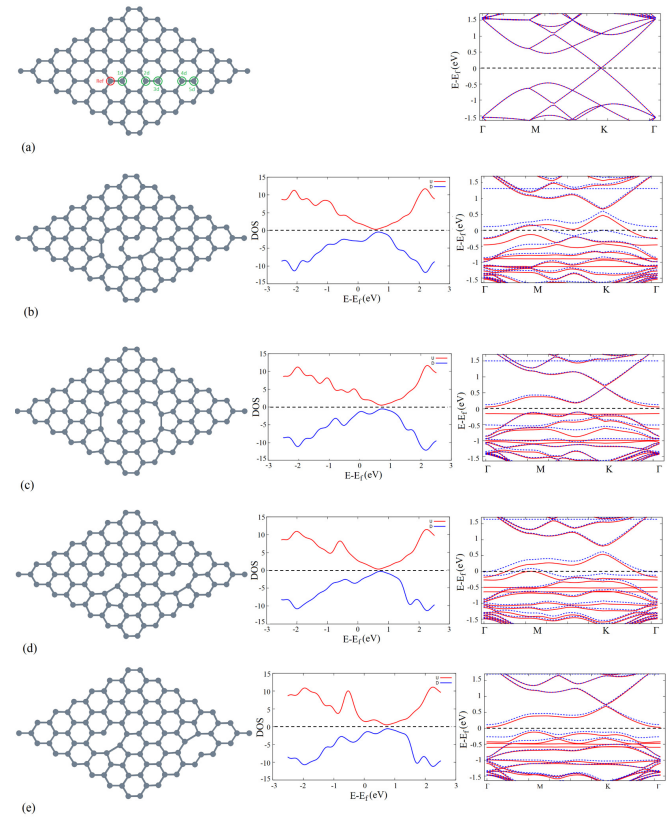


FIG. 2: (a) Band structure of a pristine graphene monolayer, and a supercell of two-vacancy states, produced by removing a reference (red circle) and second C -atoms 1, 2, 3, and 4 (green circles), located correspondingly in the 1d, 2d, 3d, and 4d interatomic distances with d being equal to $C - C$ bond length. The relaxed supercell, DOS, and the band-structure of two vacancies located at (b) one atomic distance (1d), (c) 2d-, (d) 3d-, and (e) 4d-interatomic distance.

ergy smaller than that for mono-vacancy (see, Table I), is suggested⁶⁰ to be more stable, $5-8-5$ DV is responsible for migration of DV. *Ab-initio* calculations in⁶⁰ show that subsequent transformations of $555-777$ DV into $5-8-5$ then $5-7-7-5$ and again $5-8-5$ DV create finally $555-777$ DV, which differs from the initial one by rotation. $5-8-5$ DV transforms to two sequential $5-7-7-5$ metastable DV structures, which differ each other by rotation of heptagons and shifting of pentagons. The metastable $5-7-7-5$ DV structure finally turns to stable $5-8-5$ DV, the position of which differs slightly from the position of initial $5-8-5$ DV.

In order to see clearly the differences between a di-

vacancy and other possible two-vacancy structures the latter are created, as it is seen from Fig. 2, in four different positions within the supercell, belonging both to the same or to different sublattices. Note that study of two-vacancies problem is instructive one in order to understand Lieb's rule and contribution of the dangling bonds to the magnetization.

Two removal vacancies' positions in the supercell is depicted in Fig. 2a, where the vacancies at 'even distance' and the reference vacancy, showing by red, belong to the same sublattice (see, Figs. 2b and d), instead of the 'odd distance' vacancy and the reference vacancy belong to the different sublattices (see, Figs. 2c and e). According to the Lieb's rule, the magnetization in the first case should be finite, whereas in the second case it should be zero. The formation energies and the magnetizations of different two-vacancy topologies are presented in Table III. As it is seen from Fig. 2, all relaxed supercell structures contain two pentagon-nonagon $5-9$ defects, each of which is typical of a mono-vacancy in Fig. 1a, even when two vacancies are located in $1d$ distance. Two vacancies in larger distance do not interact practically each other, and the formation energies as well as the magnetizations become approximately two times higher than that of a mono-vacancy. All the two-vacancy structures (in Fig. 2) except a di-vacancy in Fig. 1b have dangling bonds. Consequently, the local DOS of DV for spin-up and spin-down states, shown in Fig. 1b correspondingly by red (above zero) and blue (below zero) curves, coincides completely at each points. The local DOS corresponding to two opposite spin polarizations for all other vacancy configurations, presented in Figs. 2, differ each other due to existence of the dangling bonds. The magnetization of all these configurations becomes non-zero irrespective to which sublattice the vacancies belong. This fact show that the Lieb's rule seems to violate for a graphene mono-layer, and the magnetic moment of the supercell with several vacancies is determined with the number of the dangling bonds but not with the difference of the number of atoms in each sublattices. The band structures of di-vacancy and all other two-vacancy states are presented correspondingly in Fig. 1b and Figs. 2b, c, d, e. It is necessary to pay attention to the fact that two-vacancies (including the DV) generate quasi-localized state (see, the band structures in Fig. 1b and Figs. 2c, e) when they belong to the different sublattices, and instead two-vacancies generate an extended state (see the band structures in Figs. 2b, d) when they belong to the same sublattices. Furthermore, the band structures, corresponding to spin-up and spin-down states, coincide each other only in the presence of the di-vacancy due to absence of a dangling bond. All other two-vacancy structures contain dangling bonds, resulting in a splitting of opposite spin-polarized states in the band structures.

In order to create a tri-vacancy structure we remove three nearest-neighboring carbon atoms belonging to one hexagon in the center of the supercell. The relaxed struc-

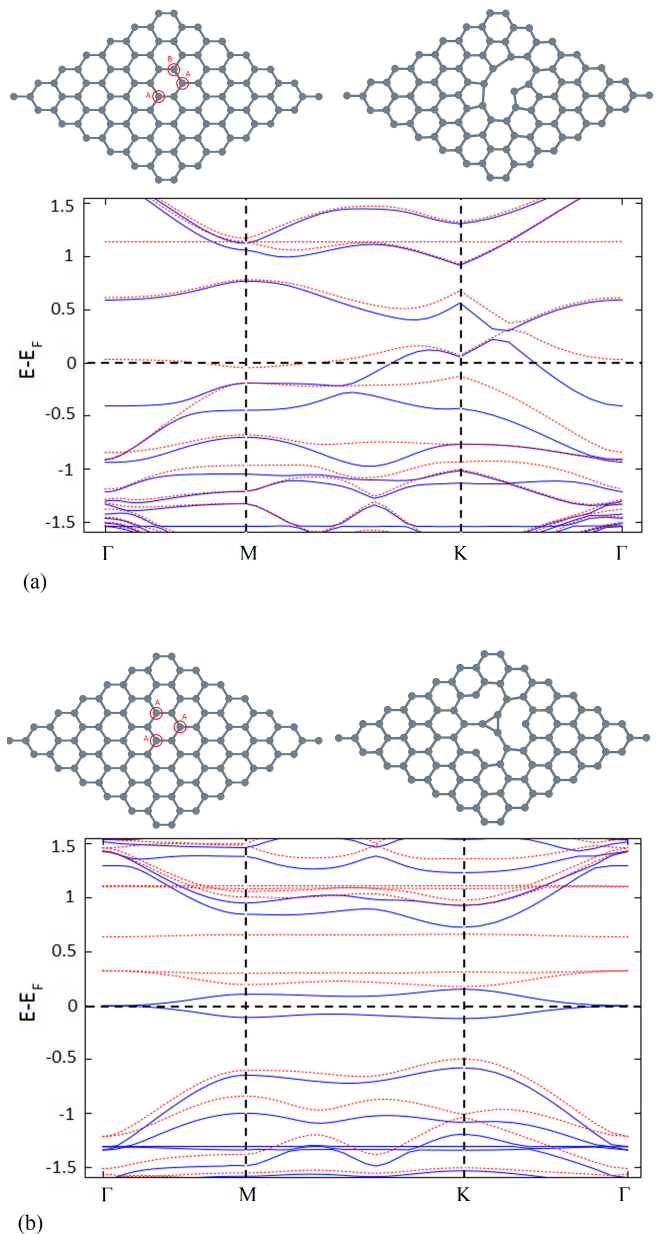


FIG. 3: Two other possible structures for three-vacancy defect, where not all three vacancies are bounded each others in difference from the tri-vacancy structure in Fig. 1c with three bounded removal C -atoms.

ture, depicted in Fig. 1c, creates $55-10$ defect consisting of two pentagons and one decagon. The band structure and DOS of a graphene with a tri-vacancy defect is presented in Fig. 1c. Tri-vacancy introduces four defect levels, two of which narrows back the band gap and other two levels cross the Fermi level, transforming the graphene to metallic state. Apart from the tri-vacancy defect two other structures with three vacancies are considered, which are produced (i) by removing two nearest-neighboring carbon atoms in a hexagon but the third

TABLE III: The formation energy and the total spin polarization for two vacancies in different positions shown in Figs. 2.

Distance (in interatomic dist. d)	Formation energy (eV)	Spin polarization ($Q_{up} - Q_{down}$)
1d (DV)	5.76	0.0
2d	13.027	2.614
3d	13.197	2.003
4d	13.547	2.339
5d	13.435	2.016

one is located in the next-nearest to these two atoms as it is depicted in Fig. 3a, producing three pentagon and one undecagon defect, (ii) by removing three carbon atoms in a hexagon all belonging to one sublattice as it is shown in Fig. 3b, which produces three nonagon and one triangle. All these configurations with three vacancies contain dangling bonds, and therefore, reveal a magnetic moment. Nevertheless the formation energy and the magnetic moment of the tri-vacancy of *55-10* defect take the values $8.84 eV$ and $1.00 \mu_B$, correspondingly (see, Table II). The values of the formation energy and the magnetic moment for other configurations *999-3* and *555-11* are respectively $17.49eV$, $4.00\mu_B$ and $11.91eV$, $1.54\mu_B$ (see, Table II), which are much more higher than those given for tri-vacancy *55-15*. The tetra-vacancies of different configurations are depicted in Fig.4. Among of all these configurations only one structure *555-9* containing three pentagon and one nonagon defects has the minimal formation energy $7.91 eV$ and zero magnetic moment (see, Table II). The relaxed supercell and the band structure of *555-9* tetra-vacancy is depicted in Fig. 4a. The opposite spin-polarization bands of the *555-9* tetra-vacancy are highly degenerated. Furthermore, the Fermi energy in this case crosses the vacancy level yielding an extended state. Two other tetra-vacancy configurations, the relaxed supercells and the band structures of which are shown in Fig. 4b, and c, contain exactly the same defect structure *5-12-5* of two pentagons and one dodagon and have the same formation energy $\sim 11.27 eV$ and the magnetic moment $\sim 2.02 \mu_B$. The tetra-vacancy structure *55-12* of two pentagon and one dodagon defects, presented in Fig. 4d, is produced by removing four nearest-neighboring atoms in a hexagon. The same relaxed supercell with *55-12* defect is obtained by removing two nearest-neighboring atoms in one side and two similar atoms in other side of the hexagon so that these pairs are not connected each other. The formation energy and the magnetic moment of this type of defects are $13.33 eV$ and $1.99 \mu_B$ correspondingly. A small band gap is opened around the Fermi level in these configurations, the band structures of which are presented in Fig. 4b, c, and d, yielding quasi-localized states. Note that there is an imbalance of the vacancies between the sublattices A and B in the tetra-vacancy depicted in Fig. 4a, since 3 vacancies belong to one sublattice and only one vacancy

belongs to other sublattice. Nevertheless, the number of vacancies located in A and B sublattices are equal each other in other three tetra-vacancy configurations of Figs. 4b, c, and d. Note that tri- and tetra-vacancy have been studied⁶¹ by coalescing a mono-vacancy to di- and tri-vacancy, correspondingly. Therefore, the obtained morphologies correspond to those drawn in Figs. 4b, c, and d with non-zero magnetic moments.

The discussion above show that SVs in a graphene are rather mobile defects, which may migrate and coalesce with other single vacancy forming a DV or with other polyvacancies even at temperatures slight higher than that of a room temperature. DVs are immobile defects at room temperature. Nevertheless they can migrate either at higher temperatures or by means of transformation to other DV modifications. The mobile defects are reincorporated into the crystal structure at dislocations, grain boundaries and other defect sinks or at the crystal external surfaces.

Summarizing all these calculation results, one can conclude that (i) among of the vacancy clusters with even vacancies there is at least one cluster where the dangling bond is absent. The magnetic moment of such vacancy cluster is zero, and the formation energy of such cluster is less than those of all other clusters with the equal number of the vacancies; (ii) among of the clusters with odd vacancies there is at least one configuration which contains only one dangling bond. The formation energy of such cluster is minimal among of all clusters with equal number of vacancies, and the magnetic moment of this vacancy cluster in $\sim 1 \mu_B$; (iii) the vacancy induced magnetic moment of the graphene does not obey the Lieb's rule, which states that the magnetization of a bi-lattice structure is determined with the difference of the atomic number in the sub-lattices. Our calculations show that the vacancy induced magnetic moment is determined with the number of the dangling bonds in the structure; (iv) the formation energy of N vacancies, coalesced into a single hole is less than the other aggregations of N vacancies with several pieces. Therefore, mono-vacancies in a graphene migrate and are collected in a hole-like structure with lowest in energy. In a real crystal, migration of mobile vacancies takes place toward an extended defects existing in the structure like grain boundary, dislocation or a sample edge, segregating from the parent structure and healing the crystal.

IV. SEGREGATION OF VACANCIES AND HEALING EFFECT IN GRAPHENE

Recent transmission electron microscopy (TEM)⁶²⁻⁶⁵ and scanning tunneling microscopy experiments⁶⁶ reveal defects and vacancies and their migration in graphene with atomic resolution. Irradiation of a graphene sample with high energy electrons or ions creates homogeneously distributed single vacancies. The migration barrier of a single vacancy in graphene was calculated by several

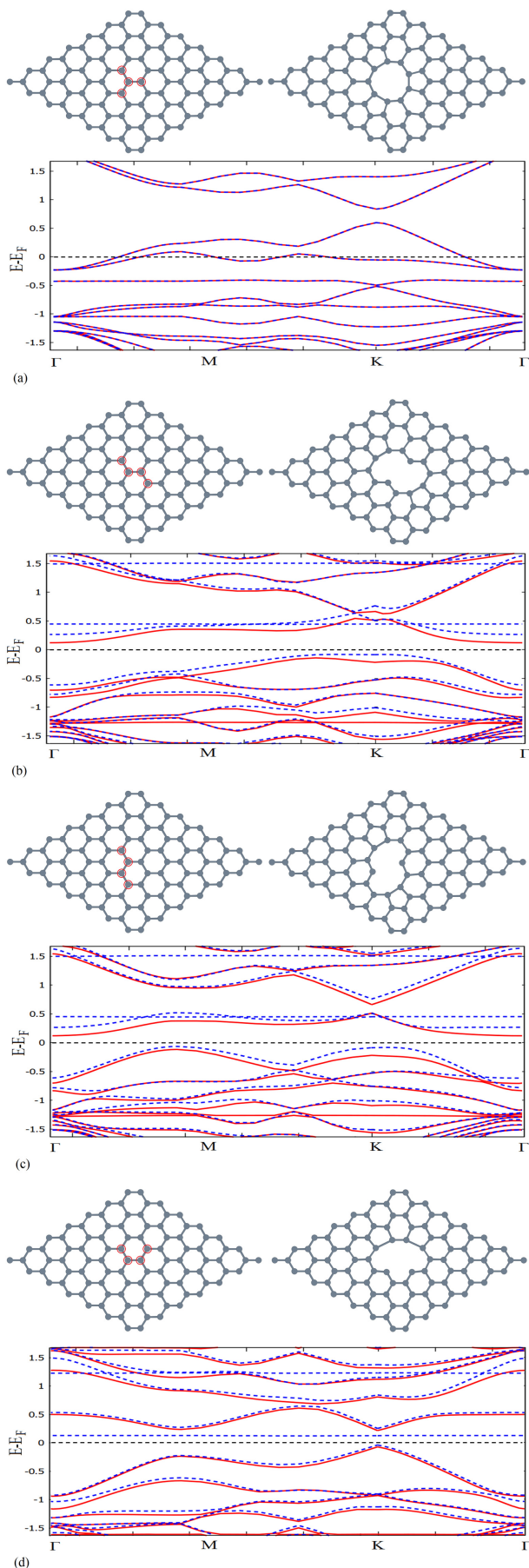


FIG. 4: Different topologies of four vacancies in the supercell; their band structures, formation energies and the magnetic moments.

groups^{56,57,61} yielding about 1.3 eV. We examined that a formation energy of divacancy is lower than that of two isolated monovacancies. This fact has been shown in other works^{67,68} too. Therefore, the single isolated vacancy is rather mobile, and it can migrate and has a tendency to coalesce either with other single vacancy to form a divacancy⁶⁷ or with an extended defect like grain boundary, dislocation or the sample edge. The migration energy of a DV was calculated⁵⁶ to be around of 7 eV, which is much higher than that presented above for a single vacancy. Nevertheless, migration of the divacancies has been recently reported in Girit et al. work⁶⁴, where the real-time dynamics of carbon atoms were visualized in a defective graphene using the aberration-corrected TEM technique. The subatomic resolution of the TEM images allows us to observe a formation of divacancies and their diffusion in the crystalline structure. In the previous Section we calculated a formation energy of three vacancies (in one hexagon) and a four (connected) vacancies in the supercell, which can be realized in 3 and 4 different forms, depicted in Figs. 1, 3 and 4, correspondingly. Among of all these configurations only tri-vacancy (Fig. 1c) and tetra-vacancy (Fig. 4a) have minimal formation energy and minimal magnetization, allowing the vacancies to inosculate into a big cluster.

Irradiation produces point defects, which are distributed randomly throughout the sample. The flux of atoms and defects causes a buildup or depletion of alloying defects and/or vacancies in the vicinity of dislocations, grain boundaries or the crystal surface.

In order to study dynamics of atoms and defects in a graphene, resulting in their redistribution, we use extensive kinetic model of segregation in dilute alloys^{47,48,50,51}. The possibility that impurities or alloying elements might segregate and form second phases at internal surfaces such as voids or on the external surfaces during irradiation was reported in many publications^{41–46,49–51} and was first confirmed experimentally in a high-purity 18Cr – 8Ni – 1Si stainless steel during in situ bombardment in a high-voltage electron microscope^{42,43}, in heavy-ion bombarded vanadium^{44,45}, stainless steels⁴⁶, and in nickel binary alloys⁴⁹. The vacancies in the graphene layer are considered to be in a thermal equilibrium state during diffusion process, which imposes that the thermal equilibrium concentration of the vacancies is reached in a time considerably smaller than the diffusion time. A diffusion process is characterized by the concentration gradient of the carbon atoms or the vacancies, which is the only factor of the nonequilibrium process.

As a consequence of irradiation of the graphene with ions (e.g., with fluorine) or with high-energy protons and carbon (C^{4+}) ions³⁸, the local concentrations of C_A carbon and C_B alloying atoms as well as the local concentrations of C_V vacancies and C_i interstitials change according to the following continuity equations^{46,49–51} for

atoms or defects fluxes,

$$\frac{\partial C_A}{\partial t} = \nabla [D_A \alpha \nabla C_A + S C_A (d_{Ai} \nabla C_i - d_{AV} \nabla C_V)], \quad (1)$$

$$\frac{\partial C_V}{\partial t} = \nabla [-(d_{AV} - d_{BV}) \alpha S C_V \nabla C_A + D_V \nabla C_V] + K_0 - R, \quad (2)$$

$$\frac{\partial C_i}{\partial t} = \nabla [(d_{Ai} - d_{Bi}) \alpha S C_i \nabla C_A + D_i \nabla C_i] + K_0 - R \quad (3)$$

where K_0 and R are correspondingly the rates of production and recombination of vacancies and interstitials by irradiation, S is the average surface area of two-dimensional (2D) sample under investigation. The first term on the right-hand side of Eq. (1) is the atom (carbon atom and adatom in our case) fluxes induced by the chemical-composition gradient, the second and third terms are the atom fluxes driven by the interstitial and vacancy gradients, respectively. The defect fluxes represented by the right-hand-side of Eqs. (2) and (3) for vacancies and interstitials are driven by the A - and B -atom concentration gradients and by their own gradients, respectively. The total diffusion coefficients for the various species D_A , D_B or D_V , D_i are written as⁵¹,

$$\begin{aligned} D_A &= d_{AV} N_V + d_{Ai} N_i, \\ D_V &= d_{AV} N_A + d_{BV} N_B, \\ D_i &= d_{Ai} N_A + d_{Bi} N_B, \end{aligned} \quad (4)$$

$$(5)$$

where N_A (N_B) and N_V (N_i) are the A (B)-atom fraction and the atomic fraction of vacancies (of interstitials), respectively. Two terms in the expression of D_A are the partial diffusivity coefficients of A -atoms respectively via N_V atomic fraction of vacancies and via N_i atomic fraction of interstitials. The diffusivity coefficients d_{AV} and d_{Ai} are given as⁶⁹,

$$d_{AV} = \frac{1}{4} b_V^2 z_V \nu_{AV}, \quad d_{Ai} = \frac{1}{4} b_i^2 z_i \nu_{Ai}, \quad (6)$$

where ν_{AV} (ν_{Ai}) is the jump frequency for the exchange of a given A -atom-vacancy (A -atom-interstitial) pair, b_V (b_i) and z_V (z_i) are correspondingly the jump distance and the coordination number for a vacancy (for an interstitial). The similar parameters can be defined for a diffusion of B -atoms via interstitials and vacancies. The equation for the element B is omitted according to the relation $C_B = 1 - C_A$. The thermodynamic factor α in expressions (1)-(3)

$$\alpha = 1 + \frac{\partial \ln \gamma_A}{\partial \ln N_A} = 1 + \frac{\partial \ln \gamma_B}{\partial \ln N_B}, \quad (7)$$

takes care of the difference between the chemical potential gradient⁵¹, which is the true driving force for the diffusion of A - and B -atoms, and the concentration gradient. γ_A and γ_B are the activity coefficients. The thermodynamic factor deviates from unity for non-ideal solutions.

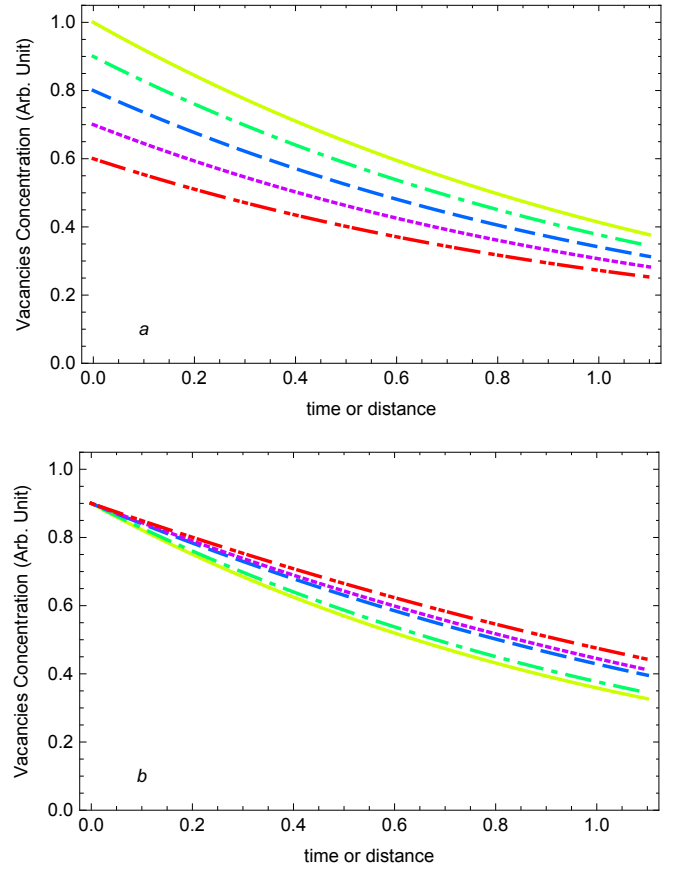


FIG. 5: Distribution of the vacancy concentration with time (or in space) in a sample with dimensionless length $L = 7$ (a) at fixed value of $\alpha = 1.2$ and for $N_{0V} = 1.0$ solid (yellow) curve, $N_{0V} = 0.9$ dot-dashed (green) curve, $N_{0V} = 0.8$ dashed (blue) curve, $N_{0V} = 0.7$ dotted (violet) curve, and $N_{0V} = 0.6$ double dot-dashed (red) curve; and (b) at fixed value of $N_{0V} = 0.9$ and for $\alpha = 1.1$ solid (yellow) curve, $\alpha = 1.5$ dashed (blue) curve, $\alpha = 1.6$ dotted (violet) curve, and $\alpha = 1.8$ double dot-dashed (red) curve.

The coupled system of equations (1)-(3) is a set of the *non-linear partial differential equations* in two variables, which was solved numerically in many works^{42-46,49-51}. In order to study dynamics of the vacancy concentration in a graphene, we simplify expressions (1)-(3), written for one-dimensional case, by ignoring the interstitials ($C_i = 0$) and alloying atoms ($C_B = 0$), also by converting the surface concentrations C into the atomic fractions N according to the relationship $N_A = S C_A$ and $N_V = S C_V$. We assume that an irradiation of the system is finished, and further generation of the vacancies and defects is stopped, $R_0 = 0$ and $K = 0$. By turning to new dimensionless variables $\rho = x/b_V$ for the spatial coordinate and $\tau = z_V \nu_{AV} t / 4$ for the time, the equations for the dimensionless atomic fraction $N_A = C_A S$ and $N_V = C_V S$ read

as,

$$\frac{\partial N_A}{\partial \tau} = \frac{\partial}{\partial \rho} \left[\alpha N_V \frac{\partial N_A}{\partial \rho} - N_A \frac{\partial N_V}{\partial \rho} \right], \quad (8)$$

$$\frac{\partial N_V}{\partial \tau} = \frac{\partial}{\partial \rho} \left[N_A \frac{\partial N_V}{\partial \rho} - \alpha N_V \frac{\partial N_A}{\partial \rho} \right]. \quad (9)$$

Migration of a vacancy throughout the crystal is realized by hopping of a carbon atom over the vacancy. Therefore, the time evolutions of the atoms and the vacancies are opposite each other. Equations (8) and (9) are second-order non-linear coupled equations for $N_A(\rho, \tau)$ and $N_V(\rho, \tau)$. Furthermore, the atomic fractions for carbon atoms $N_A(\rho, \tau)$ and for vacancies $N_V(\rho, \tau)$ are linked according to

$$N_A(\rho, \tau) = 1 - N_V(\rho, \tau), \quad (10)$$

since the total concentrations of carbon atoms and vacancies at arbitrary point is conserved in the absence of interstitials as well as of production and recombination of the vacancies under irradiation.

We introduce new coordinate $\xi = \rho + \tau$ and demand that N_A and N_V depend only on ξ , so that $N_A(\rho, \tau) = N_A(\xi)$ and $N_V(\rho, \tau) = N_V(\xi)$. It is worthy to note that such transformation resembles the *soliton* transformation for the Korteweg-de Vries (KdV) equation⁷⁰. Then Eqs. (8) and (9) can be written under this assumption and the condition (10) in the following form,

$$\frac{\partial}{\partial \xi} \left\{ \alpha(1 - N_A) \frac{\partial N_A(\xi)}{\partial \xi} + N_A \frac{\partial N_A(\xi)}{\partial \xi} - N_A \right\} = 0 \quad (11)$$

$$\frac{\partial}{\partial \xi} \left\{ (1 - N_V) \frac{\partial N_V(\xi)}{\partial \xi} + \alpha N_V \frac{\partial N_V(\xi)}{\partial \xi} + N_V \right\} = 0 \quad (12)$$

Further we will study only the Equation (12) for the vacancy fraction, and the solution for $N_A(\xi)$ can be determined according to Eq.(10). Integration of Eq. (12) yields

$$(1 - N_V) \frac{\partial N_V(\xi)}{\partial \xi} + \alpha N_V(\xi) \frac{\partial N_V(\xi)}{\partial \xi} - N_V = N_0 \quad (13)$$

This equation (13) is once more integrated yielding,

$$\begin{aligned} & [1 + (1 - \alpha)N_0] \ln \left| \frac{N_A(\xi) + N_0}{N_0} \right| - \\ & (1 - \alpha) [N_A(\xi) + N_0] = \xi + N_1. \end{aligned} \quad (14)$$

The constants N_0 and N_1 have to be determined from the boundary conditions. A 1D sample of the dimensionless length L is assumed to be free of the internal defects and sinks, so that segregation could occur only to the edge. The conditions are imposed to the half of the sample because of the symmetry of the problem. The vacancy is assumed to be created at $t = 0$ at the center of the sample $x = 0$ with concentration of $N_V(x = 0, t = 0) \equiv N_{0V} = \exp(-E_V/k_B T)$, where E_V is the formation

energy of a vacancy. At the same time, the vacancy concentration and flux at the boundary $\xi = L/2$ is given as $N_V(\xi = L/2) = [1 - \exp(-E_V/k_B T)]/L = (1 - N_{0V})/L$ and $\left. \frac{\partial N_V}{\partial \xi} \right|_{\xi=L/2} = 0$. These conditions yield,

$$N_0 = \frac{N_{0V} - 1}{L} = \frac{1}{L} \left\{ \exp\left(-\frac{E_V}{k_B T}\right) - 1 \right\}; \quad (15)$$

$$\begin{aligned} N_1 = & \left[1 - (1 - \alpha) \frac{1 - N_{0V}}{L} \right] \ln \left| \frac{N_{0V} + \frac{N_{0V} - 1}{L}}{\frac{N_{0V} - 1}{L} + N_{0V}} \right| - \\ & (1 - \alpha) \left(N_{0V} + \frac{N_{0V} - 1}{L} \right). \end{aligned} \quad (16)$$

Finally, the time- /coordinate-evolution of $N_V(\xi = x/b_V + z_V \nu_{AV} t/4)$ reads as

$$\begin{aligned} & \left[1 + (1 - \alpha) \frac{N_{0V} - 1}{L} \right] \ln \left| \frac{N_V(x, t) + \frac{N_{0V} - 1}{L}}{N_{0V} + \frac{N_{0V} - 1}{L}} \right| - \\ & (1 - \alpha) [N_V(x, t) - N_{0V}] = \frac{x}{b_V} + \frac{1}{4} z_V \nu_{AV} t. \end{aligned} \quad (17)$$

Fig. 5 shows the vacancy density dependence on time or coordinate. We assume that the vacancy concentration of $N_{0V}(T) = e^{-\frac{E_V}{k_B T}}$ is created at $t = 0$ at the middle of the sample $x = 0$ with length L by irradiation. Irradiation is stopped just at $t = 0$, and the system is relaxed to an equilibrium state by migration of the carbon atoms over the vacancies. Fig. 5a shows migration of the vacancy concentration, created at $x = 0$ point at $t = 0$ with different concentration C_{0V} for fixed parameter α , with time, so that the vacancy concentration at $x = 0$ decreases with time and segregates to the boundary of the sample. Figure 5b displays the same dependence that is in Fig. 5a for fixed value of $C_{0V}(T)$ but for different values of α .

V. CONCLUSIONS

Considerable attention has been paid recently to understand magnetism of a single layered graphene. In this work we studied influence of the vacancies on the magnetic properties and healing effects of a graphene. Our *ab-initio* DFT investigations of mono-, di-, tri- and tetra-vacancy in the single-layer graphene show that the formation energy of many-vacancies is lower when the vacancies coalesce together forming a big cluster (hole) instead of homogeneously distribution over the structure as single vacancies. Furthermore, the formation energy is minimal when the σ -bonds, appearing in the process of vacancy creation, rebind each other reducing the dangling bonds to the minimal number in the internal edge of the hole. In this case, a contribution to the magnetic moment yields the dangling bonds in the internal edge of the hole, the number of which is much less than the total number of the vacancies.

The process of clustering of the vacancies is similar to the segregation process in binary compounds. In a crystalline binary bulk (3D) compound the segregation may result in separation of the structure into two coexistent crystalline substructures or into film on the host crystal in the compound. Such a picture of a clustering and forming the holes under irradiation, instead of homogeneous creation of vacancies in a graphene, seems to be a result of two-dimensional character of the structure and absence of the off-diagonal long range order (ODLRO)⁷¹.

ODLRO fails in the two-dimensional (2D) crystals due to the Mermin-Wagner theorem^{71,72}. Characterizing the order in the crystalline structure by the order parameter $\Delta(\mathbf{r})$ at a point \mathbf{r} , ODLRO is determined by the correlator $\langle \Delta(\mathbf{r})\Delta(\mathbf{r}') \rangle$ which behaves as $\langle \Delta(\mathbf{r})\Delta(\mathbf{r}') \rangle = C \exp\left(-\frac{\xi^{(3D)}}{|\mathbf{r}-\mathbf{r}'|^\alpha}\right)$ for 3D structures, where $C > 0$ and $\alpha > 1$ are constants, $\xi^{(3D)}$ is the coherence length, and as $\langle \Delta(\mathbf{r})\Delta(\mathbf{r}') \rangle = \left(\frac{\xi^{(2D)}}{|\mathbf{r}-\mathbf{r}'|}\right)^\beta$ for 2D systems, where $\beta > 1$ is a constant and $\xi^{(2D)}$ is the coherence length. Although the correlator in 3D system saturates at long distance $\lim_{|\mathbf{r}-\mathbf{r}'| \rightarrow \infty} \langle \Delta(\mathbf{r})\Delta(\mathbf{r}') \rangle \rightarrow C$, it vanishes in 2D structures. Since long wave-length fluctuations destroy the ODLRO in 2D systems⁷². The vacancies in the graphene correlate according to power-like interaction. Therefore the vacancies form a cluster (hole) by joining each other, which competes with the 2D graphene structure. The vacancy induced magnetism in the graphene is determined by the dangling bonds on the edge of the hole. On the

other hand the hole structure is energetically favorable when the dangling bonds on the edge rebind each other reducing the magnetization to a minimal value. The graphene structure is destroyed by reaching the holes size to a critical value.

A graphene structure with randomly distributed vacancies can be considered as kinetically frozen-in thermodynamically non-equilibrium states. A clustering of the vacancies into holes in a graphene sheet can be understood as a segregation of the structure, which means a partitioning of atomic or molecular constituents into macroscopic regions of different compositions. In order to understand segregation of vacancies in a graphene sheet we study analytically dynamics of the carbon atoms and vacancies by means of non-linear diffusion equations. Exact solution of these KdV-like non-linear equations shows that the vacancies, created in the middle of the sample diffuse to the boundary of the sample resulting a self-healing of the graphene layer.

Acknowledgments

The reported study was funded by the Science Development Foundation under the President of the Republic Azerbaijan-Grant No EIF-KETPL-2-2015-1(25)-56/01/1, and partially by Azerbaijan-JINR collaboration.

-
- ¹ K. S. Novoselov, A. K. Geim, S. V. Morozov, D. Jiang, Y. Zhang, S. V. Dubonos, I. V. Grigoreva, and A. A. Firsov, *Science* **306**, 666 (2004).
 - ² A. K. Geim, *Science* **324**, 1530 (2009).
 - ³ K. S. Novoselov, Z. Jiang, Y. Zhang, S. V. Morozov, H. L. Stormer, U. Zeitler, J. C. Maan, G. S. Boebinger, P. Kim, and A. K. Geim, *Science* **315**, 1379 (2007).
 - ⁴ J. H. Warner, M. H. Rummel, L. Ge, T. Gemming, B. Montanari, N. M. Harrison, B. Büchner, and G. A. D. Briggs, *Nature Nanotech.* **4**, 500 (2009).
 - ⁵ R. Zhao, J. Zhuang, Z. Liang, T. Yan, and F. Ding, *Nanoscale* **7**, 8315 (2015).
 - ⁶ R. Zan, U. Bangert, Q. Ramasse, and K. S. Novoselov, *J. Phys. Chem. Lett.* **3**, 953 (2011).
 - ⁷ Q. M. Ramasse, R. Zan, U. Bangert, D. W. Boukhvalov, Y.-W. Son, and K. S. Novoselov, *ACS Nano* **6**, 4063 (2012).
 - ⁸ B. W. Smith and D. E. Luzzi, *J. Appl. Phys.* **90**, 3509 (2001).
 - ⁹ R. Zan, Q. M. Ramasse, U. Bangert, and K. S. Novoselov, *Nano Lett.* **12**, 3936 (2012).
 - ¹⁰ J. Chen, T. Shi, T. Cai, T. Xu, L. Sun, X. Wu, and D. Yu, *Appl. Phys. Lett.* **102**, 103107 (2013).
 - ¹¹ X. Gao, L. Liu, S. Irle, and S. Nagase, *Angew. Chem., Int. Ed.*, **49**, 3200 (2010).
 - ¹² L. Wang, F. Yan, H. L. W. Chan, and F. Ding, *Nanoscale* **4**, 7489 (2012).
 - ¹³ A. Santana, A. M. Popov, and E. Bichoutskaia, *Chem. Phys. Lett.* **557**, 80 (2013).
 - ¹⁴ T. Botari, R. Paupitz, P. A. Autrero, and D. S. Galvao, *Carbon* **99**, 302 (2016).
 - ¹⁵ Z. Liu, Y.-C. Lin, C.-C. Lu, C.-H. Yeh, P.-W. Chiu, S. Iijima, and K. Suenaga, *Nat. Commun.* **5**, 4055 (2014).
 - ¹⁶ V. O. Özçelik, H. H. Gürel, and S. Çıraçı, *Phys. Rev. B* **88**, 045440 (2013).
 - ¹⁷ P. T. Araujo, M. Terrones, and M. S. Dresselhaus, *Materialstoday* **15**, 98 (2012).
 - ¹⁸ G. Mestl, N. I. Maksimova, N. Keller, V. V. Roddatis, and R. Schlögl, *Angew. Chem., Int. Ed. Engl.* **40**, 2066 (2001).
 - ¹⁹ J. M. Carlsson and M. Scheffer, *Phys. Rev. Lett.* **96**, 046806 (2006).
 - ²⁰ F. G. M. M. Ugeda, I. Brihuega, F. Guinea, and J. M. Gomez-Rodriguez, *Phys. Rev. Lett.* **104**, 096804 (2010).
 - ²¹ Y. Wang, Y. Huang, Y. Song, X. Zhang, Y. Ma, J. Liang, and Y. Chen, *Nano Lett.* **9**, 220 (2009).
 - ²² J. Červenka, M. I. Katsnelson, and C. F. J. Flipse, *Nature Physics* **5**, 840 (2009).
 - ²³ O. V. Yazyev and L. Helm, *Phys. Rev. B* **75**, 125408 (2007).
 - ²⁴ J. J. Palacios and F. Ynduráin, *Phys. Rev. B* **85**, 245443 (2012).
 - ²⁵ S. Chakrabarty, A. H. M. Abdul Wassey, R. Thara, and G. P. Das, *AIP Advances* **5**, 087163 (2015).
 - ²⁶ O. V. Yazyev, *Rep. Prog. Phys.* **73**, 056501 (2010).
 - ²⁷ Y. Zhang, S. Talapatra, S. Kar, R. Vajtai, S. K. Nayak,

- and P. M. Ajayan, Phys. Rev. Lett. **99**, 107201 (2007).
- ²⁸ F. Banhart, J. Kotakoski, and A. Krasheninnikov, ACS Nano **9**, 26 (2011).
- ²⁹ Y. Ma, P. O. Lehtinen, A. S. Foster, and R. M. Nieminen, New J. Phys. **6**, 68 (2004).
- ³⁰ X. Y. Cui, R. K. Zheng, Z. W. Liu, L. Li, B. Delley, C. Stampfi, and S. P. Ringer, Phys. Rev. B **84**, 125410 (2011).
- ³¹ V. M. Pereira, J. M. B. Lopes dos Santos, A. H. Castro Neto, *Modeling disorder in graphene*. Phys. Rev. B **77**, 115109 (2008).
- ³² V. M. Pereira, F. Guinea, J. M. B. Lopes dos Santos, N. M. R. Peres, and A. H. Castro Neto, Phys. Rev. Lett. **96**, 036801 (2006).
- ³³ P. Ruffieux, O. Gröning, P. Schwaller, L. Schlapbach, and P. Gröning, Phys. Rev. Lett. **84**, 4910 (2000).
- ³⁴ H. A. Mizes and J. S. Foster, Science **244**, 559 (1989).
- ³⁵ P. Ruffieux, M. Melle-Franco, O. Gröning, M. Biemann, F. Zerbetto, and P. Gröning, Phys. Rev. B **71**, 153403 (2005).
- ³⁶ E. H. Lieb, Phys. Rev. Lett. **62**, 1201 (1989).
- ³⁷ M. Slota, A. Keerthi, W. K. Myers, E. Tret'yakov, M. Baumgarten, A. Ardavan, H. Sadeghi, C. J. Lambert, A. Narita, K. Müller, and L. Bogani, Nature **557**, 691 (2018).
- ³⁸ R. R. Nair, M. Sepioni, I.-Ling Tsai, O. Lehtinen, J. Keinonen, A. V. Krasheninnikov, T. Thomson, A. K. Geim, and I. V. Grigorieva, Nature Phys. **8**, 199 (2012).
- ³⁹ R. R. Nair, I.-L. Tsai, M. Sepioni, O. Lehtinen, J. Keinonen, A. V. Krasheninnikov, A. H. Castro Neto, M. I. Katsnelson, A. K. Geim, and I. V. Grigorieva, Nature Commun. **4**, 2010 (2013).
- ⁴⁰ M. Sepioni, R. R. Nair, S. Rablen, J. Narayanan, F. Tuna, R. Winpenny, A. K. Geim, and I. V. Grigorieva, Phys. Rev. Lett. **105**, 207205 (2010).
- ⁴¹ T. R. Anthony, AEC Symp. Series, *Radiation Induced Voids in Metals and Alloys*, Conf-701601, Ed. J. W. Corbett and L.C. Ianiello, 630 (1972).
- ⁴² P. R. Okamoto, S. D. Harkness, and J. J. Laidler, ANS Trans. **16**, 70 (1973).
- ⁴³ P. R. Okamoto and S.D. Harkness, Quarterly Prog. Report, HEDL-TME-72-144 (August, September, October 1972).
- ⁴⁴ P. R. Okamoto, A. T. Santhanam, H. Wiedersich, and A. Taylor, Nucl. Technology **22**, 45 (1974).
- ⁴⁵ A. T. Santhanam, A. Taylor, S. D. Harkness, proc. Conf. Defects and Defect Clusters in BCC metals and their Alloys, Ed. R. J. Arsenaut, Nucl. Mat. **18**, 302 (1972).
- ⁴⁶ P. R. Okamoto and H. Wiedersich, J. Nucl. Math. **53**, 336 (1974).
- ⁴⁷ R. A. Johnson and N. Q. Lam, Phys. Rev. B **13**, 4364 (1976).
- ⁴⁸ R. A. Johnson and N. Q. Lam, Phys. Rev. B **15**, 1794 (1977).
- ⁴⁹ L. E. Rehn, P. R. Okamoto, D. I. Potter, and H. Wiedersich, J. Nucl. Math. **74**, 242 (1978).
- ⁵⁰ R. A. Johnson and N. Q. Lam, J. Nucl. Mater. **69&70**, 424 (1978).
- ⁵¹ H. Wiedersich, P. R. Okamoto, and N. Q. Lam, J. Nucl. Mater. **83**, 98 (1979).
- ⁵² P. Ordejón, E. A. Artacho, and J. M. Soler, Phys. Rev. B **53**, R10441 (1996).
- ⁵³ J. M. Soler, E. Artacho, J. D. Gale, A. Garcia, J. Junquera, P. Ordejón, and D. Sanchez-Portal, J. Phys. C: Condens. Matter **14**, 2745 (2002).
- ⁵⁴ J. P. Perdew, K. Burke, and M. Ernzerhof, Phys. Rev. Lett. **77**, 3865 (1996).
- ⁵⁵ H. J. Monkhorst and J. D. Pack, Phys. Rev. B **13**, 5188 (1976).
- ⁵⁶ A. A. El-Barbary, R. H. Telling, C. P. Ewels, M. I. Heggie, and P. R. Briddon, Phys. Rev. B **68**, 144107 (2003).
- ⁵⁷ A. V. Krasheninnikov, P. O. Lehtinen, A. S. Foster, and R. M. Nieminen, Chem. Phys. Lett. **418**, 132 (2006).
- ⁵⁸ P. A. Thrower and R. M. Mayer, Phys. Stat. Solidi A **47**, 11 (1978).
- ⁵⁹ A. J. Stone and D. J. Wales, Chem. Phys. Lett. **128**, 501 (1986).
- ⁶⁰ Y. Kim, J. Ihm, E. Yoon, and G.-D. Lee, Phys. Rev. B **84**, 075445 (2011).
- ⁶¹ T. Trevelyan, C. D. Latham, M. I. Heggie, P. R. Briddon, and M. J. Rayson, Nanoscale, **6**, 2978-2986 (2014).
- ⁶² A. Hashimoto, K. Suenaga, A. Gloter, K. Urita, and S. Iijima, Nature **430**, 870 (2004).
- ⁶³ J. C. Meyer, C. Kisielowski, R. Erni, M. D. Rossel, M. F. Grommie, and A. Zettl, Nano Lett. **8**, 3582 (2008).
- ⁶⁴ C. Ö. Girit, J. C. Meyer, R. Erni, M. D. Rossel, C. Kisielowski, L. Yang, C.-H. Park, M. F. Grommie, M. L. Cohen, S. G. Louie, and A. Zettl, Science **323**, 1705 (2009).
- ⁶⁵ O. Lehtinen, I. -L. Tsai, R. Jalil, R. R. Nair, J. Keinonen, U. Kaiser, and I. V. Grigorieva, Nanoscale **6**, 6569 (2014).
- ⁶⁶ L. Tapasztó, G. Dobrik, P. Nemez-Incze, G. Vertesy, P. Lambin, and L. P. Biró, Phys. Rev. B **78**, 233407 (2008).
- ⁶⁷ G. D. Lee, C. Z. Wang, E. Yoon, N. M. Hwang, D. Y. Kim, and K. M. Ho, Phys. Rev. Lett. **95**, 205501 (2005).
- ⁶⁸ M. Saito, K. Yamashita, and T. Oda, Jpn. J. Appl. Phys. **46**, L1185 (2007).
- ⁶⁹ The multiplayer $1/6$ in the front of d_{AV} and d_{Ai} in Ref. [51], which is valid for $3D$ systems is replaced by $1/4$ according to Fick's diffusion coefficient for $2D$ systems.
- ⁷⁰ P. G. Drazin and R. S. Johnson, *Solitons: An Introduction*, Cambridge text in Applied Mathematics, Cambridge, 1989.
- ⁷¹ N. D. Mermin and H. Wagner, Phys. Rev. Lett. **17**, 1133 (1966).
- ⁷² T. M. Rice, Phys. Rev. **140**, A1889 (1965).